*Desalination and Water Treatment*
www.deswater.com

doi: 10.5004/dwt.2022.28888

273 (2022) 270–280
October

# Effective removal of reactive blue 198 from aqueous solutions by hybrid chitosan-PANI/$Fe_3O_4$@C composite based on rice husk

Trong Tang Nguyen[a], Thanh Phuc Tran[a], Thi Hong Anh Nguyen[b], Xuan Thang Cao[a], Van Cuong Nguyen[a,*]

[a]*Faculty of Chemical Engineering, Industrial University of Ho Chi Minh City, 12 Nguyen Van Bao St., Go Vap Dist., Ho Chi Minh City, 700000, Vietnam, emails: nvc@iuh.edu.vn (V.C. Nguyen), nguyentrongtang@iuh.edu.vn (T.T. Nguyen), tranthanhphuc123@gmail.com (T.P. Tran), caoxuanthang@iuh.edu.vn (X.T. Cao)*
[b]*Faculty of Chemical Engineering, Ho Chi Minh City University of Food Industry, 140 Le Trong Tan St., Tay Thanh Ward, Tan Phu Dist., Ho Chi Minh City, 700000, Vietnam, email: anhnth@hufi.edu.vn (T.H.A. Nguyen)*

Received 10 April 2022; Accepted 20 August 2022

**ABSTRACT**

In this study, we have successfully synthesized magnetic carbon composite by utilizing eco-friendly and biocompatible chitosan (CS), polyaniline (PANI) and rice husk. First rice husk was converted into magnetic carbon ($Fe_3O_4$@C) and mixed in the dissolution of chitosan. Finally, aniline dissolved in HCl was added into the resulting mixture to initiate the copolymerization process in the presence of sodium thiosulfate affording CS-PANI/$Fe_3O_4$@C composite. SEM, EDX, TGA, FT-IR, VSM, and XRD analytical techniques confirmed the successful formation of the composite. The synthesized CS-PANI/$Fe_3O_4$@C composite was tested as a magnetically separable adsorbent to remove reactive blue 198 (RB198) dye from an aqueous solution. The experimental results showed that the composite possessed adsorption efficiency > 90% for an initial concentration of RB198 dye of 100 mg/L. Moreover, we investigated the effects of concentration, time, pH, and temperature on the adsorption efficiency of the composite as well as the kinetics of the process. The maximum adsorption capacities were calculated to be 108.7, 121.9, and 123.5 mg/g at 293, 303, and 313 K respectively. Moreover, the composite can be easily regenerated by soaking in basic solution followed by washing with water. CS-PANI/$Fe_3O_4$@C was recycled up to four consequent cycles and retained ~70% dye adsorption capacity.

*Keywords:* Adsorption; Chitosan; Polyaniline; Magnetic carbon; Rice husk

## 1. Introduction

Water is the source of life and therefore needs to be preserved, recycled, and purified. A significant amount of water is being used in various industries such as textiles, leather, paper, rubber, printing, and plastic etc. In fact, a medium-sized textile manufacturer consumes approximately 1.6 million L/d of water and approximately 200 L of water are required to produce 1 kg of textile fabric [1,2]. Moreover, the daily life activities (washing, bathing, and cleaning) also contribute to the water pollution. This polluted water is discharged into the environment without any treatment causing the serious environmental problems. Therefore, water treatment has piqued the interest of research scholars all over the world. Among the various water pollutants, dyes are one of the main active contaminants widely used to color a variety of products in various industries and thus produce a huge amount of wastewater as effluent. Based on the data, approximately 0.8 million tons of dyes were synthesized and more than

* Corresponding author.

10,000 different types of dyes and pigments are estimated to be used globally each year [1–3]. Unfortunately, approximately 15% of dyes were discharged into the water during the dyeing process [3]. Waste water having high concentration of dye pollutant poses a significant risk not only to the ecological system but also to humans [4,5]. The dye polluted water prevents the penetration of light and thus interferes in photosynthesis process and causes problem to aquatic organisms. Moreover, humans may experience allergic reactions, carcinogenic, mutagenic effects, dermatitis, rhinitis, kidney disease and reproductive damage due to the unwanted absorption of these dyes [6,7]. Therefore, a number of methods have been developed including advance oxidation, coagulation, coagulation–flocculation, precipitation, adsorption, and biological treatment to remove dyes from industrial effluent [5,8–10]. Although, every method has its own advantages and disadvantages, the adsorption method is being widely used to treat wastewater. It is comparatively simple, effective and low-cost method for not only to remove the dyes but also heavy metals [4]. A series of materials have been used as adsorbents or as a precursor to synthesize the adsorbents such as activated carbon [11–13], ordered mesoporous carbon [14,15], zeolites, limestone, natural clay [16], industrial and agricultural waste [17], nano and polymer materials [4,18,19]. However, the bio-based adsorbent, biosorbents, are the materials of interest for the preparation of future adsorbent because of their non-toxic, inexpensive, easily availability, biodegradable and sustainable nature [20–22].

Biomaterials (chitosan, bagasse, husk etc.) are the naturally occurring biopolymers with exciting chemical and physical properties. Particularly, chitosan has mainly amino and hydroxyl functional groups, and positive charge that are generated while deacetylation of chitin. Chitosan and its derivatives have been used in a variety of important applications, including metal ion adsorption, dye removal, drug delivery, and pharmaceutical applications [23–27]. Metal ions can be absorbed by chitosan and its derivatives via chelating due to the presence of a large number of hydroxyl and amino groups [28–30]. However, the main challenge associated with using chitosan for the synthesis adsorbent is its dissolution in acidic solutions and low mechanical strength. Consequently, physical and chemical modifications have been accomplished to improve its applicability and reusability. The synthesis of nanocomposite by integrating chitosan with some other materials (carbon, biopolymers, organic polymers etc.) is an effective strategy to enhance its adsorption capacity. In fact, the maximum adsorption capacity of the magnetic chitosan/active charcoal composite towards methylene blue (MB) and reactive blue 4 (RB4) was calculated to be 500 and 250 mg/g, respectively [31]. Polyaniline (PANI), also known as a conducting polymer, has picked the interest of researchers due to its conducting behavior and appealing physicochemical properties. PANI and PANI-based adsorbents were widely used in wastewater treatment to remove heavy metals and organic pollutants [32–34].

Accordingly, the goal of current study is to synthesize a magnetic separable carbon composite utilizing rice husks, an agricultural waste source, chitosan and polyaniline with improved adsorption capacity and reusability. The prepared composite was then tested as bio-sorbent for the removal of reactive blue 198 (RB198) from aqueous solution.

## 2. Materials and methods

### 2.1. Materials

Rice husk was collected from local rice mills in Vietnam. Thanh Cong textile dying company provided C.I. Reactive Blue 198 (RB198) ($M_w$ = 1304.80 g/mol, $\lambda_{max}$ = 604 nm) dye. Aniline was procured from Merck (Germany). We performed deacetylation of chitin to obtain chitosan in our laboratory. Iron(III) chloride hexahydrate ($FeCl_3{\cdot}6H_2O$) and iron(II) chloride tetrahydrate ($FeCl_2{\cdot}4H_2O$) were indented from TCI Chemical (Japan).

### 2.2. Preparation of carbon from rice husk

Rice husk was washed with distilled water to remove dust and foreign objects, and dried at 105°C until constant weight. 5 g of washed rice husk was then annealed at 650°C under nitrogen atmosphere for 1.0 h in a ceramic crucible to obtain the black color powdered material. The synthesized material was subjected to 200 mL of NaOH at 80°C to remove $SiO_2$ based impurities and then filtered, washed with double distilled water until neutral pH and dried at 105°C [35,36].

### 2.3. Preparation of magnetic carbon ($Fe_3O_4$@C)

Magnetic carbon was synthesized by dissolving 0.01 mol of iron(III) chloride hexahydrate ($FeCl_3{\cdot}6H_2O$) and 0.005 mol of iron(II) chloride tetrahydrate ($FeCl_2{\cdot}4H_2O$) in 150 mL of distilled water and agitating at room temperature for 10 min to obtain the yellow-orange color solution. Carbon from rice husk was added to this solution under continues stirring followed by drop wise addition of 1 M $NH_4OH$ solution until the pH 12 while maintaining the temperature between 70°C–80°C. The color of solution first changed from orange-yellow to brown-black and finally to black color indicating the formation of $Fe_3O_4$ species. The resulting mixture was incubated at 160°C for 6 h in the absence of oxygen. The solid material was filtered, washed with deionized water until neutral pH and dried at 100°C to obtain the $Fe_3O_4$@C [37].

### 2.4. Synthesis of CS-PANI/$Fe_3O_4$@C composite

Firstly, 1.0% chitosan dissolution was prepared by dissolving 2.0 g of chitosan in 200 mL of 1% acetic acid solution and the resulting solution was magnetically stirred for 2.0 h at room temperature. A mixture of 2.0 g of $Fe_3O_4$@C and 2.0 g of aniline dissolve in 1 M HCl was added to the dissolution of chitosan under stirring. Finally, equivmolar amount of ammonium persulfate ($(NH_4)_2S_2O_8$) was added to the resulting mixture and stirring was continued for another 6 h at 5°C. The color of reaction mixture turned to deep blue indicating the occurrence of polymerization reaction between chitosan and aniline. Reaction was quenched by adding 1 M NaOH to achieve pH 7–8 and the solid material was then filtered, rinsed with double distilled water, and lyophilized to yield a CS-PANI/$Fe_3O_4$@C-1 composite [34].

The other composites were prepared by taking CS-PANI and $Fe_3O_4$@C in 1:2 and 2:1 weight ratio, and the composites were referred as CS-PANI/$Fe_3O_4$@C-0.5 and CS-PANI/$Fe_3O_4$@C-2, respectively.

### 2.5. Characterizations

The functional group of the composite was characterized using Fourier-transform infrared spectroscopy (FT-IR, Tensor 27-Bruker, Germany) with wavelengths spanning from 4,000 to 400 $cm^{-1}$. The morphology of the composite was examined by scanning electron microscopy (SEM, Hitachi S-4800, and JSM-IT200, Tokyo, Japan). The XRD was measured on LabX XRD-6100, Shimadzu, Japan from 10° to 80° in 2θ steps using Cu-K$\alpha$ radiation. A TA TGA Pt1600 device was used to determine the thermal properties of the samples (TA Instruments, Linseis, North, USA).

### 2.6. Adsorption study

In order to examine the adsorption effectiveness of RB198 onto the CS-PANI/$Fe_3O_4$@C composite, a series of tests were carried out by using 0.05 g of adsorbent and 50 mL of RB198 solution with concentrations ranging from 20 to 150 mg/L for the time intervals ranging from 5 to 150 min with a shaking speed of 150 rpm. Moreover, the effect of temperature on the adsorption efficiency of the composite was investigated for the concentration of 50 mg/L at different temperatures of 293, 303, and 313 K for 5 to 120 min. Furthermore, the effect of pH was investigated at 3, 5, 7, and 9 using 0.05 g of adsorbent and 50 mL of RB198 solution (50 mg/L). Finally, the effect of the presence of foreign ions on the adsorption efficiency of the composite was investigated using 0.05 g of adsorbent and 50 mL of RB198 solution (50 mg/L) containing the cations ($Na^+$, $K^+$, and $Mg^{2+}$) and anions ($Cl^-$, $NO_3^-$, and $SO_4^{2-}$). The concentrations of cations and anions were taken in between 0.1 and 1 mol/L. The adsorbent was easily separated from the solution by applying an external magnate in all of the studies. A UV-Vis spectrophotometer (Thermo Scientific Evolution 600) was used to detect the concentration of remaining RB198 dye at a wavelength of 604 nm. The experiment was repeated three times and an average was taken as final value.

The removal efficiency was calculated by Eq. (1).

$$H\% = \frac{C_0 - C_t}{C_0} \times 100\% \tag{1}$$

where $C_0$ is initial concentration of RB198 (mg/L) and $C_t$ is concentration of RB198 at various interval of time (mg/L).

Adsorption capacity was calculated by Eq. (2):

$$q = \frac{\left(C_0 - C_t\right) \times V \times 10^{-3}}{m} \tag{2}$$

where $q$ is adsorption capacity (mg/g). $V$ and $m$ are volume of RB198 (L) and amount of adsorbent (g), respectively.

## 3. Result and discussion

### 3.1. Surface mophology and structural characterization

The morphology of the prepared composites was examined using a scanning electron microscope (Fig. 1). Irregular round or oval pores of varying sizes are clearly visible on the surface of CS-PANI/$Fe_3O_4$@C nanocomposites. However, carbon and magnetic carbon surface displayed completely different morphology with no sign of pores (Fig. 1a and b). Moreover, surface morphology

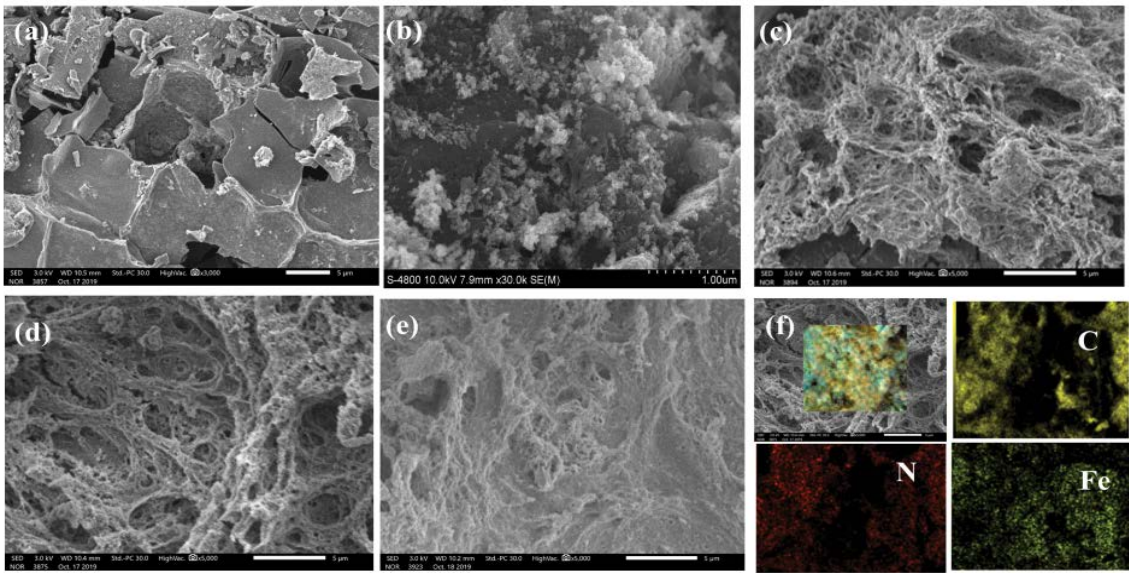


Fig. 1. SEM images of (a) carbon, (b) $Fe_3O_4$@C, (c) CS-PANI/$Fe_3O_4$@C-0.5, (d) CS-PANI/$Fe_3O_4$@C-1, (e) CS-PANI/$Fe_3O_4$@C-2 and (f) EDX image of CS-PANI/$Fe_3O_4$@C-1.

in terms of pore size and shape found to vary with the composition ratios of chitosan-PANI and $Fe_3O_4$@C indicating composition dependent morphological behavior (Fig. 1c–e). EDX spectra of composites revealed the presence of C, N, O, and Fe elements, proving the active role of chitosan, polyaniline, activated carbon and $Fe_3O_4$ in the synthesis of nanocomposite (Fig. 1f).

FT-IR results of all prepared nanocomposites are shown in Fig. 2. Stretching vibrations for the O–H and N–H groups are at 3,407 and 2,926 $cm^{-1}$, respectively. The prominent absorption peaks at 2,918 and 2,887 $cm^{-1}$ are attributed to the symmetric and asymmetric stretching vibrations of the –CH and $–CH_2$ groups, respectively. Moreover, absorption peak at 1,587 $cm^{-1}$ corresponds to the bending vibration of the N–H groups (amide II). The other peaks at 1,423 and 1,375 $cm^{-1}$ could be ascribed to C–H bending vibrations of the $–CH_2$ and $–CH_3$ groups, respectively. The peak at 1,150 $cm^{-1}$ is assigned to an asymmetric stretching vibration of C–O–C bonds. The bands formed at 1,066 and 1,028 $cm^{-1}$ are caused by stretching vibrations of C–O [38]. Furthermore, all samples have distinct bands at 1,508 and 1,309 $cm^{-1}$ corresponding to C=C– and C–N– stretching as a result of PANI benzenoid rings, respectively [39]. Additionally, all composites displayed a peak around 568 $cm^{-1}$ due to the stretching vibration of Fe–O in $Fe_3O_4$ [27].

The XRD pattern of CS-PANI/$Fe_3O_4$@C composites showed characteristic reflections at 2θ = 36°, 43°, 53°, and 63° which correspond to the Miller indices of the cubic crystal plane of $Fe_3O_4$ (220), (400), (422), and (400), respectively. Moreover, broad and overlapping peaks at 2θ = 19.8°, 23.1°, and 25.2° attribute to the characteristic peaks of chitosan, carbon, and polyaniline, respectively. Polyaniline and chitosan are semi-crystalline with a low degree of crystallinity as indicated by the broad peaks (Fig. S1) [40,41]. The vibrating sample magnetometer (VSM) was used to investigate the magnetic properties of the composites at room temperature. The VSM result demonstrates that saturation magnetizations ($M_s$) for CS-PANI/$Fe_3O_4$@C and $Fe_3O_4$@C are 0.008 and 0.036 emu/g, respectively (Fig. S2). The coating of nonmagnetic polymer around the magnetic $Fe_3O_4$@C may explain the decrease in magnetization saturation of CS-PANI/$Fe_3O_4$@C [42,43]. However, it was demonstrated that the material can be easily separated from aqueous solutions using an external magnetic force after dye adsorption process.

The thermal stability of the CS-PANI/$Fe_3O_4$@C composite is determined using TGA (Fig. 3). TGA curves for composites show three step decompositions at the temperatures of 100°C, 270°C, and 550°C. The first weight loss in between room temperature to 200°C for the CS-PANI/$Fe_3O_4$@C-1, CS-PANI/$Fe_3O_4$@C-0.5, and CS-PANI/$Fe_3O_4$@C-2 composites was 3.4%, 7.1%, and 8.9%, respectively. The weight loss is proportional to the amount of absorbed and interfacial water in the respective composites. The further weight loss was 16.9%, 18.4%, and 33.8% in the range of 200°C to 350°C and corresponds to the dehydration of the saccharide rings and the breakage of the C–O–C glucoside linkages in the main chain of chitosan. However, weight loss was highest for CS-PANI/$Fe_3O_4$@C-2, and lowest for CS-PANI/$Fe_3O_4$@C-1 indicating 1:1 weight ratio of CS-PANI and $Fe_3O_4$@C leads to higher thermal stability. Weight of the nanocomposites continues to drop to 58.8, 53.8 and 65.6% corresponding to the CS-PANI/$Fe_3O_4$@C-1, CS-PANI/$Fe_3O_4$@C-0.5, and CS-PANI/$Fe_3O_4$@C-2, respectively, on further increasing the temperature to 675°C. In this case, weight loss was higher for CS-PANI/$Fe_3O_4$@C-1 rather than CS–PANI/$Fe_3O_4$@C-0.5. It could be due to the thermal breakdown and degradation of remaining chitosan and PANI associted moeites which are less in CS–PANi/$Fe_3O_4$@C-0.5 [44]. At 800°C, the residual contents of the CS-PANI/$Fe_3O_4$@C-0.5, CS-PANI/$Fe_3O_4$@C-1, and CS-PANI/$Fe_3O_4$@C-2 composites were 17.2, 12.6, and 3.5%, respectively.

The surface area and porosity of the composites were calculated by Brunauer–Emmet–Teller (BET) using the $N_2$ gas adsorption method. The results are shown in Fig. 4 and Table 1. The nature of $N_2$-adsoption and desorption curve belongs to the type-IV isotherm according to the IUPAC classification. The specific surface areas of the samples CS-PANI/$Fe_3O_4$@C-2, CS-PANI/$Fe_3O_4$@C-1, and CS-PANI/$Fe_3O_4$@C-0.5 were calculated to be 15.54, 16.28, and 11.23 $m^2/g$, respectively. It was observed that

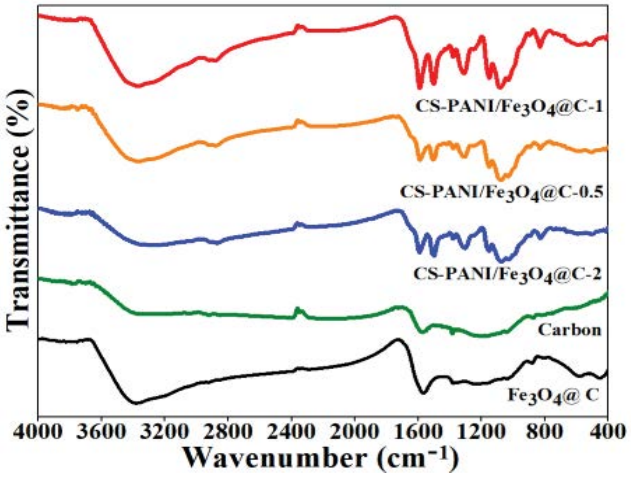


Fig. 2. FT-IR of carbon, $Fe_3O_4$@C and CS-PANI/$Fe_3O_4$@C composite.

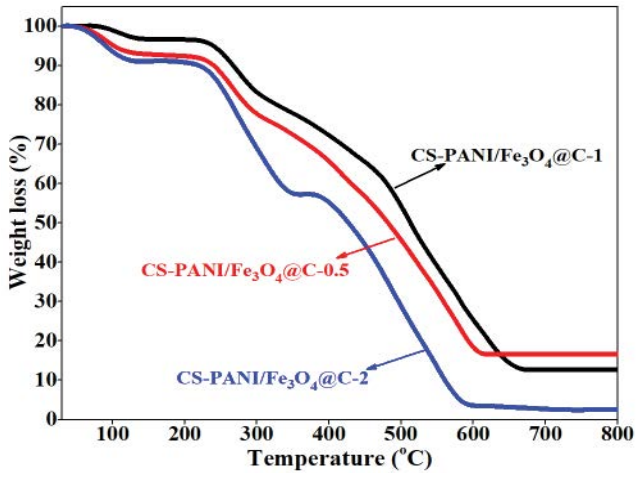


Fig. 3. TGA curve of composite CS-PANI/$Fe_3O_4$@C with various ratio of chitosan-PANI: $Fe_3O_4$@C.

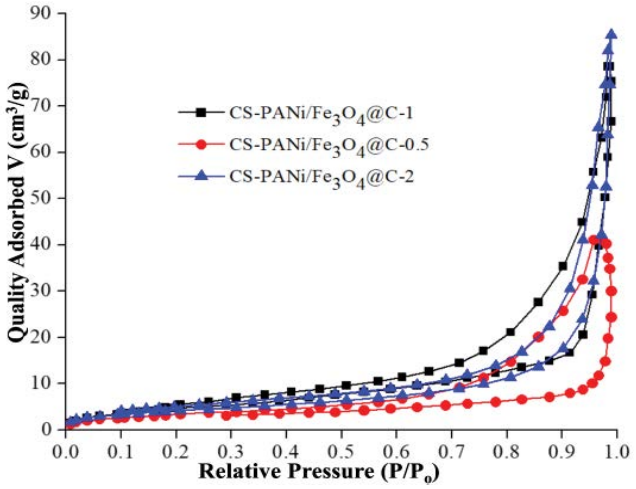


Fig. 4. Nitrogen adsorption–desorption curves of CS-PANI/$Fe_3O_4$@C.

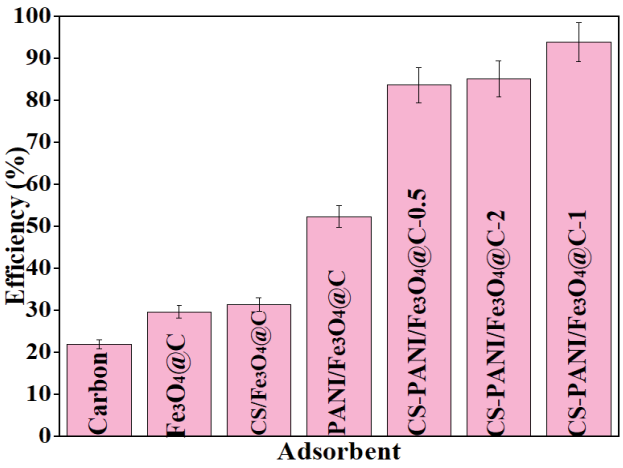


Fig. 5. The adsorption efficiency of synthesized materials towards RB198 dye solution. Condition: 0.05 g of adsorbent, 50 mL of dye (50 mg/L), 60 min.

Table 1
BET surface areas and pore volumes of composites

| Samples | BET surface areas ($m^2$/g) | Average pore size (nm) | Pore volume ($cm^3$/g) |
|---|---|---|---|
| CS-PANI/$Fe_3O_4$@C-0.5 | 11.23 | 22.61 | 0.06 |
| CS-PANI/$Fe_3O_4$@C-1 | 16.28 | 29.86 | 0.12 |
| CS-PANI/$Fe_3O_4$@C-2 | 15.54 | 34.02 | 0.13 |

average pore size increase as the concentration of chitosan and polyamine increases in composites resulting pore sizes ranging from 22.61 to 34.02 nm indicating a mesoporous structure. Similar results were also observed for chitosan-grafted-polyorthoethylaniline biocomposite [45].

### 3.2. Adsorption study of RB198 onto CS-PANI/$Fe_3O_4$@C

#### 3.2.1. Effect of various materials and weight ratio of chitosan-PANI and $Fe_3O_4$@C

Various materials (chitosan/$Fe_3O_4$@C, PANI/$Fe_3O_4$@C, CS-PANI/$Fe_3O_4$@C, carbon, and $Fe_3O_4$@C) were synthesized to evaluate their adsorption capacity. The adsorption experiments were conducted by taking 0.05 g of each materials and 50 mL of RB198 solution (50 mg/L) for 60 min. Fig. 5 depicts the effect of several materials on the adsorption percentage RB198 dye. Carbon, $Fe_3O_4$@C, chitosan/$Fe_3O_4$@C, and PANI/$Fe_3O_4$@C displayed lower dye removal efficiency than CS-PANI/$Fe_3O_4$@C. These results indicated that chitosan-grafted polyamine significantly enhanced the removal efficiency of CS-PANI/$Fe_3O_4$@C materials due to increased porosity and strong interaction between the positive charge of the chitosan-grafted polyaniline polymer and the anionic dye RB198 [46]. The CS-PANI/$Fe_3O_4$@C-1 was the most effective and displayed over 94% dye removal efficiency. The results are in good agreement with the BET analysis, that is, highest specific surface area giving higher adsorption efficiency. Subsequently, CS-PANI/$Fe_3O_4$@C-1 was chosen for further investigation.

#### 3.2.2. Effect of adsorbent dose and pH

The effect of adsorbent amount for RB198 dye removal was investigated by taking different amounts (0.010, 0.025, 0.05, 0.075, and 0.1 g). The percentage of dye adsorption increased at higher dosages of adsorbent (data not shown). The dye removal efficiency was 75.2% for 0.01 g which increased to 93.5% for 0.05 g of adsorbent. However, further increasing the amount of adsorbent from 0.05 to 0.1 g improved the removal efficiency slightly. Thus high surface area and availably of active sites can help to increase the dye adsorption efficiency [41]. Furthermore, dye removal efficiency was investigated at different pH values (3–9). It was observed that the removal efficiency was declined from 92.6% to 45.6% when the pH was increased from 3 to 9. Consequently, high adsorption efficiency was determined at low pH due to the protonation of the amino group producing the positively charged surface of the composite. The electrostatic interaction was thus improved between the negatively charged dye and the positively charged surface of the composite. Protons preferentially bonded to the nitrogen atoms of amine and imine groups of chitosan and PANI at low pH values leading the positive charges of composite surfaces [41]. On the other hand, amino group prone to be deprotonated at high pH thus lowering the electrostatic interaction between dye molecules and the composite surface. Additionally, the synthesized CS-PANI $Fe_3O_4$@C composite has a zero charge point at about pH 5.5. Accordingly, the composites possess net negative charges at pH > 5.5 and positive charges at pH < 5.5. The better adsorption capacity of CS-PANI $Fe_3O_4$@C under acidic environment is in agreement with point of zero charge explanation.

#### 3.2.3. Effect of initial dye concentration and contact time

The influence of initial concentration of RB198 dye and contact time on adsorption efficiency of the adsorbent were examined while varying the contact time from 5 to 150 min and the results are shown in Fig. 6a. The adsorption efficiency gradually decreased as the initial concentration of

RB198 was increased from 20 to 150 mg/L. The adsorption efficiency was 94.8% for the value of 20 mg/L in 120 min. It reduced to 84.3% when the concentration increased to 150 mg/L in same time. Moreover, it was found that the contact time influenced the adsorption efficiency significantly. Strong adsorption was observed during the first 30 min due to rapid surface adsorption and removal efficiency reached to 54% and 87% at initial concentration of 150 and 20 mg/mL respectively. The adsorption efficiency was found to gradually rise as the contact time was reached to equilibrium after 150 min. Additionally, UV-Vis spectra demonstrated the absorbance intensity diminishes as contact time increases (Fig. 6b). The quick adsorption of RB198 dye on chitosan–PANI/$Fe_3O_4$@C indicated that it was physically adsorption [31]. The faster migration of dye molecules to the significant number of adsorption sites of the composite can explain the excellent removal efficiency of RB198 dye at low concentrations [46]. The removal efficiency was lowered at higher initial concentrations due to the occupancy of all the active sites thus restricting the further absorption of dye molecules. Furthermore, steric repulsion between dye molecules might cause the adsorption process slow down and thus lowering the removal efficiency [41,47]. Similar results were observed when Congo red (CR) was applied to L-cysteine adorned with a reduced graphene oxide/polyaniline composite [48].

### 3.2.4. *Effect of interfering ions*

Foreign ions are commonly found in the waste water of textile industry. Therefore, researchers have explored the influence of foreign ions on adsorption capacity of adsorbents. The presence of cations in solution of RB198 dye had no effect on the adsorption capacity of chitosan-PANI/$Fe_3O_4$@C composite as demonstrated in Fig. 7a. However, the anions had a considerable impact on the adsorption process (Fig. 7b). Further raising the anions concentration reduces removal efficiency of chitosan-PANI/$Fe_3O_4$@C composite. When the RB198 solution was comprised with the

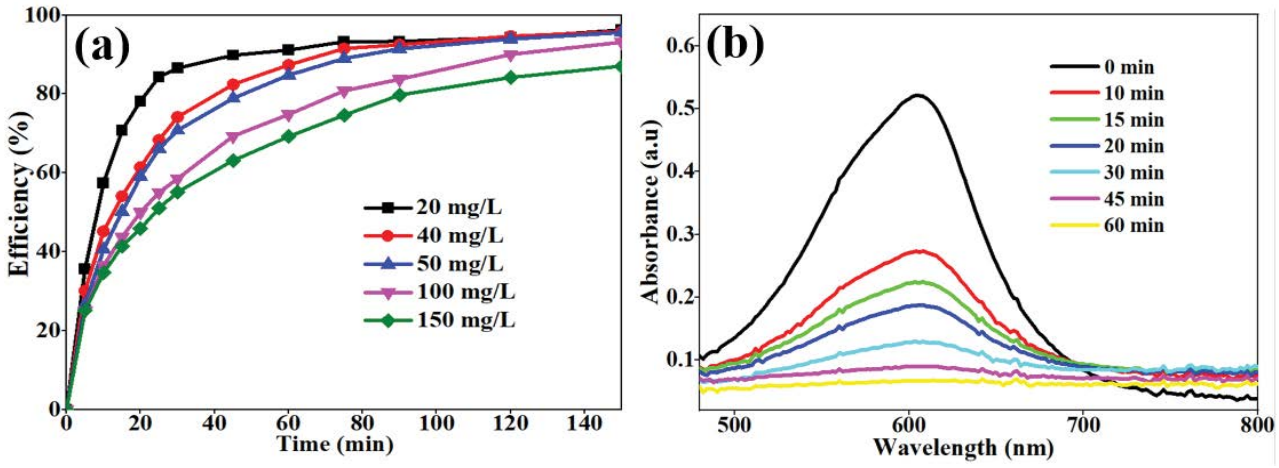


Fig. 6. The influence of the initial concentration of RB198 dye and contact time to the adsorption efficiency of CS-PANI/$Fe_3O_4$@C (a) and absorbance curve towards RB198 dye solution (50 mg/L) (b). Condition: 0.05 g of adsorbent.

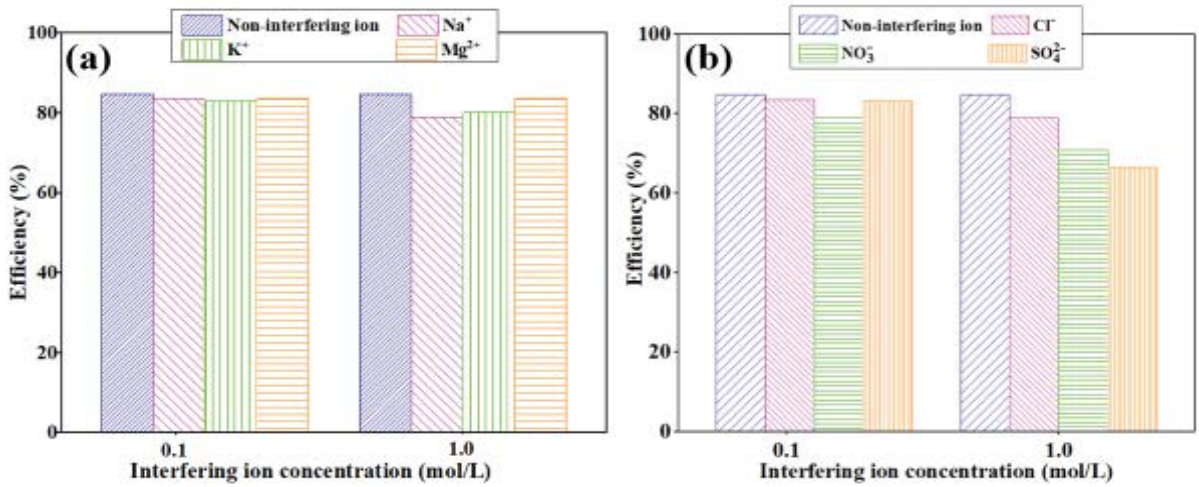


Fig. 7. Effect of interfering ions to the adsorption efficiency of CS-PANI/$Fe_3O_4$@C towards RB198 dye solution.

$Cl^-$, $NO_3^-$, $SO_4^{2-}$ anions, the removal efficiency of chitosan–PANI/$Fe_3O_4$@C composite dropped by 10%, 14%, and 20%, respectively. Anions and anionic dye molecules have the same negative charge, therefore they compete each other for adsorption on the positively charged adsorption sites of the composites [47].

### 3.3. Adsorption isotherms

Adsorption isotherms were studied by taking different initial concentrations of RB198 dye ranging from 20 to 150 mg/L at 293, 303, and 313 K with adsorbent weight of 0.05 g. The Langmuir, Freundlich, and Dubinin-Radushkevich isothermal models were used to investigate the adsorption process. Eqs. (3)–(5) describe the Langmuir, Freundlich, and Dubinin-Radushkevich isothermal adsorption models, respectively.

$$\text{Langmuir: } q_e = \frac{q_m \times K_L \times C_e}{1 + K_L \times C_e} \tag{3}$$

where $C_e$ (mg/L) is the concentration of the RB198 dye at the equilibrium, $q_e$ (mg/g) is the adsorption capacity at the equilibration, $q_m$ (mg/g) is the maximum adsorption capacity of the adsorbent, and $K_L$ is the Langmuir adsorption equilibrium constant.

$$\text{Freundlich: } q_e = K_F \times C_e^{1/n} \tag{4}$$

where $K_F$ is Freundlich equilibrium constant and $n$ is intensity of adsorption, which characterizes the energetic heterogeneity of the adsorption surface.

$$\text{Dubinin} - \text{Radushkevich: } q_e = Q_{D-R} \times e^{\left(-\beta_{D-R}\varepsilon^2\right)} \tag{5}$$

where $Q_{(D-R)}$ (mg/g) denotes the maximum adsorption capacity, $\beta_{(D-R)}$ is the isotherm constant (mol²/J²), $T$ is the temperature of the solution (K), $R$ is the universal gas constant (8.314 J/mol·K), and $E$ (kJ/mol) is the value of the average adsorption energy.

Table 2 displays the calculated parameters. The relationship between composite concentration ($C_e$) and adsorption capacity ($q_e$) is depicted in Fig. 8. Langmuir ($R^2$ = 0.991) and Freundlich ($R^2$ = 0.992) isotherms fit well with experimental data of RB198 dye adsorption onto composite at 293 K. The result indicated that the adsorption process occurred in a monolayer manner. On the other hand, the Freundlich equation had higher $R^2$ values than the Langmuir equation at 303 and 313 K thus confirming the multilayer adsorption of RB198 dye on the adsorbent surface at higher temperatures. The Dubinin–Radushkevich model did not account RB198 dye adsorption onto composite surface. However, the $E$ value for the Dubinin–Radushkevich isotherm adsorption model ranged from 0.461 to 2.882 kJ/mol, indicating physical adsorption of RB198 dye [47]. Moreover, the values of $1/n$ in the Freundlich model at three different temperatures are less than 1 indicating that the chitosan-PANI/$Fe_3O_4$@C surface is heterogeneous. The maximum adsorption capacity value for monolayer adsorption at 293, 303, and 313 K was 108.7, 121.9, and 123.5 mg/g, respectively. Based on the data, the adsorption process was known to be endothermic [49,50]. Table 3 compares the adsorption capacity of CS-PANI/$Fe_3O_4$@C for RB198 dye with different adsorbents for other reactive dyes. It is evident from the results that CS-PANI/$Fe_3O_4$@C has a relatively high adsorption capacity for reactive dyes.

Table 2
Various parameters of Langmuir, Freundlich and Dubinin–Radushkevich adsorption isotherm models

| Isotherms | Parameters | | | |
|---|---|---|---|---|
| Langmuir | Temperature (K) | 293 | 303 | 313 |
| | $K_L$ (L/mg) | 0.053 | 0.057 | 0.352 |
| | $q_m$ (mg/g) | 108.69 | 121.95 | 123.46 |
| | $R^2$ | 0.991 | 0.984 | 0.974 |
| Freundlich | $n$ | 1.926 | 1.996 | 2.948 |
| | $K_F$ (mg/g)(L/mg)$^{1/n}$ | 10.4 | 12.8 | 37.0 |
| | $R^2$ | 0.992 | 0.998 | 0.992 |
| Dubinin–Radushkevich | $Q_{D-R}$ (mg/g) | 56.2 | 58.2 | 72.2 |
| | β (mol²/kJ²) | 2.353 | 1.104 | 0.060 |
| | $E$ (kJ/mol) | 0.461 | 0.673 | 2.882 |
| | $R^2$ | 0.716 | 0.653 | 0.706 |

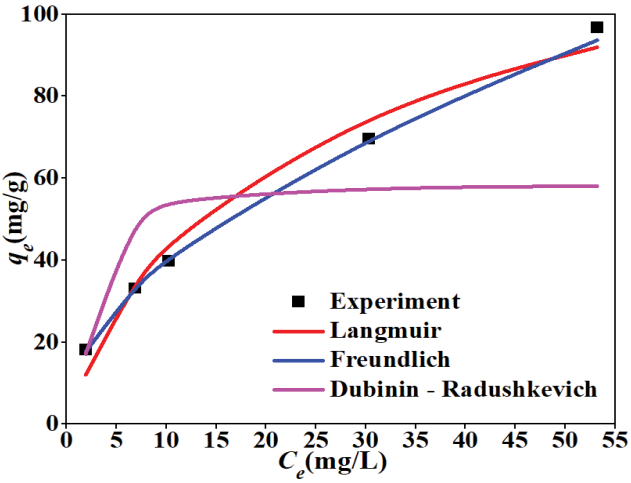


Fig. 8. Langmuir, Freundlich and Dubinin–Radushkevich models for RB198 dye adsorption onto CS-PANI/$Fe_3O_4$@C composite at 303 K.

### 3.4. Effect of temperature and thermodynamic study

The influence of temperature on the RB198 dye adsorption efficiency of composite was investigated at temperatures ranging from 283 to 313 K by taking an initial concentration of RB198 dye (50 mg/L) and adsorbent weight (0.05 g) for the period from 5 to 120 min (Fig. 9). It was observed that the adsorption efficiency of CS-PANI/$Fe_3O_4$@C increased as the temperature increased. The adsorption efficiency was 77% at 283 K for 120 min. However, the adsorption

Table 3
Comparison of the adsorption capacity of reactive dyes by various adsorbents

| Dye | Adsorbents | $q_m$ (mg/g) | References |
|---|---|---|---|
| Reactive Blue 4 | Chitosan 10B | 60.7 | [30] |
| Reactive Black 5 | ACPSD | 6.71 | [51] |
| Reactive Orange 16 | m-Cs-PVA/FA | 123.8 | [52] |
| Reactive Red 24 | SBB-$ZnO_3$ | 75.13 | [53] |
| Reactive Red 120 | QAMOPP | 344.8 | [54] |
| Reactive Red 198 | Alumina/MWCNT | 43.72 | [55] |
| Reactive Red 198 | Polyaniline/$Fe_3O_4$ | 45.45 | [56] |
| Reactive Red 198 | CS-PANi/$Fe_3O_4$ | 99.0 | [34] |
| Reactive Blue 198 | CS-PANI/$Fe_3O_4$@C | 121.9 | This study |

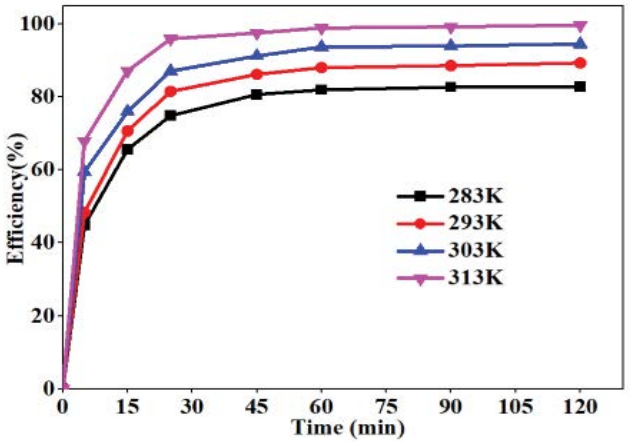


Fig. 9. Effect of temperature to adsorption efficiency of CS-PANI/$Fe_3O_4$@C towards RB198 dye. Condition: 0.05 g of adsorbent, 50 mL of dye (50 mg/L).

efficiency was increased to nearly 95% at 303 and 313 K, and above 80% at 293 K. These results revealed that RB198 adsorption onto the CS-PANI/$Fe_3O_4$@C composite is endothermic and occurs preferentially at high temperatures.

The thermodynamic parameters such as enthalpy ($\Delta H°$), entropy ($\Delta S°$) and Gibbs free energy ($\Delta G°$) for RB198 adsorption process were calculated by Langmuir isotherm model via Eqs. (6) and (7).

$$\Delta G^0 = -\mathrm{RTIn}\left(K_L\right) \tag{6}$$

$$\mathrm{In}\left(K_L\right) = \frac{\Delta S^0}{R} - \frac{\Delta H^0}{\mathrm{RT}} \tag{7}$$

where $R$ is the gas constant (8.314 J/mol·K), $T$ is the temperature (K) and $K_L$ is the Langmuir equilibrium constant (L/mol). Entropy and enthalpy are determined from the slope and intercept of the Van't Hoff of ln($K_L$) vs 1/$T$.

All of the thermodynamic parameters are calculated from Eqs. (6) and (7). The adsorption process appeared to be spontaneous and endothermic as evidenced by the negative $\Delta G°$ and posstive $\Delta H°$ (71.1 kJ/mol) values. The magnitude values of $\Delta G°$ are 3.067, 4.840 and 8.133 kJ/mol for the temperature value of 293, 300, and 313 K, repectively, showing that the adsorption process was more favorable at high temperatures [56]. The positive $\Delta S°$ (253.3 J/mol K) value demonstrates the increased degrees of freedom at the solid–liquid phase surface during the adsorption of dye RB198 dye onto CS-PANI/$Fe_3O_4$@C composite. Moreover, the adsorption of RB198 dye onto CS-PANI/$Fe_3O_4$@C was physisorption due to the $\Delta G°$ values between 0 and –20 kJ/mol [50].

### 3.5. Adsorption kinetics model

Pseudo-first-order [Eq. (9)] and pseudo-second-order [Eq. (10)] kinetic models were used to assess the experimental data to investigate the kinetics of adsoprtion.

$$\text{pseudo-first-order: } q_t = q_e\left(1 - e^{-k_1 t}\right) \tag{8}$$

$$\text{pseudo-second-order: } q_t = \frac{q_e^2 \times k_2 \times t}{1 + k_2 \times q_e \times t} \tag{9}$$

where $k_1$ (min$^{-1}$) and $k_2$ (g/mg min) are the equilibrium rate constant of pseudo-first-order and pseudo-second-order equations, respectively, and $q_t$ is the adsorption capacity at $t$ time (mg/g).

The kinetic parameters for the pseudo-first-order and pseudo-second-order are shown in Table 4 and Fig. 10. The experimental data effectively fit with first- and second-order kinetic models as evidenced by the high correlation coefficient ($R^2$ > 0.973). However, the second-order kinetic model ($R^2$ = 0.999) described the greater correlation

Table 4
Kinetic parameters for adosption of CS-PANI/$Fe_3O_4$@C towards RB198 dye

| $C_0$ (mg/L) | $q_{exp}$ (mg/g) | Pseudo-first-order | | | Pseudo-second-order | | |
|---|---|---|---|---|---|---|---|
| | | $q_{cal}$ (mg/g) | $k_1$ (1/min) | $R^2$ | $q_{cal}$ (mg/g) | $k_2$ (g/mg min) | $R^2$ |
| 40 | 39.743 | 32.443 | 0.041 | 0.993 | 40.077 | 0.0017 | 0.999 |
| 50 | 49.743 | 36.230 | 0.027 | 0.973 | 47.436 | 0.00122 | 0.999 |
| 100 | 91.663 | 73.905 | 0.028 | 0.992 | 89.741 | 0.00045 | 0.996 |
| 150 | 128.119 | 104.295 | 0.029 | 0.981 | 125.191 | 0.00035 | 0.993 |

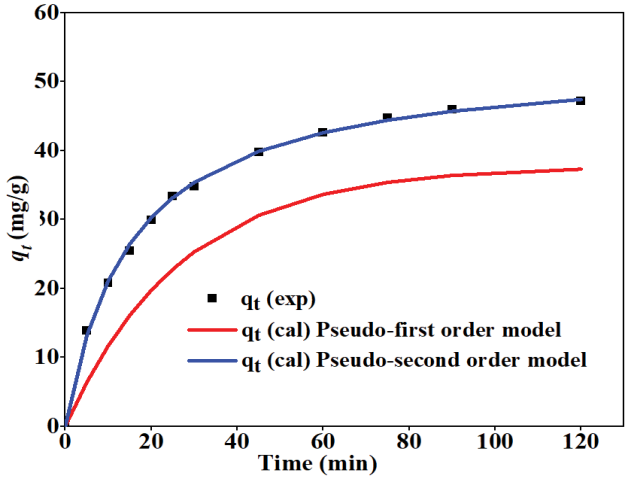


Fig. 10. Non-linear pseudo-first-order and pseudo-second-order kinetic models of CS-PANI/$Fe_3O_4$@C towards RB198 dye. Condition: 50 mL of dye (50 mg/L), 0.05 g of adsorbent.

coefficient than the first-order kinetic model ($R^2$ = 0.973). The physical adsorption process was demonstrated in the first-order kinetic model, whereas the chemical process was thought to control the second-order kinetic model. The rate controlling step of second-order kinetic model involved the chemisorption. The high $R^2$ values found for pseudo-first-order and pseudo-second-order kinetic models for all RB198 dye concentrations indicating that RB198 dye was removed from solution via a two-stage physicochemical process [46]. RB198 dye molecules adsorbed onto the pore sites in the composite caused an electrostatic contact between the positively charged composite and the negatively charged dyes during the physical adsorption stage. The adsorption rate appears to be determined by the chemical adsorption step [57,58]. Moreover, the plot of $B_t$ vs. $t$ is linear passing through the origin for 50 mg/L at 303 K (data not shown), which indicated that adsorption process is controlled by the particle diffusion.

### 3.6. Regeneration studies

The reusability of the CS-PANI/$Fe_3O_4$@C composite was tested via four desorption-adsorption cycles. The dye-loaded composite was soaked into NaOH 0.1 M for dye desorption and supernatant was decanted. The composite after dye desorption was used for the further sorption experiments. Based on the results, the removal efficiency of the adsorbent towards RB198 dye decreased from 90% to 70% after four successive cycles. The possible solution to fix the recovered dye could be its degradation (catalytic and photocatalytic) in order to avoid the further decontamination and damage to the environment.

## 4. Conclusions

In this report, we have demonstrated the facile preparation of magnetically separable CS-PANI/$Fe_3O_4$@C composite for the effective removal of RB198 dye from aqueous solution. Rice husk was used as sustainable source to produce the magnetic carbon using $Fe_3O_4$ magnetic species. Chitosan, biopolymer, and aniline were then copolymerized and in-situ supported on the magnetic carbon to enhance the adoption capacity of the resulting composite. The maximum removal efficiency of the CS-PANI/$Fe_3O_4$@C-1 composite was found to be >90%. Moreover, the maximum adsorption capacity was calculated to be 108.7, 121.9, and 123.5 mg/g at 293, 303, and 313 K respectively. Importantly, the composite CS-PANI/$Fe_3O_4$@C can be easily collected by applying the external magnetic field after the use due to its magnetic property. Moreover, the recovered composite was regenerated by desorption of dye in basic solution followed by washing with water and reused consequently up to four cycles. Based on the recycling data, the CS-PANI/$Fe_3O_4$@C-1 composite retained ~70% RB198 dye adsorption efficiency after four cycles of regeneration.

## Acknowledgment

Authors would like to thank the Industrial University of Ho Chi Minh City, Vietnam, for financial support under grant No 21.2CNHH04, and the Ho Chi Minh City University of Food Industry, Vietnam, for facility use.

## Conflicts of interests

The authors reported no conflict of interest.

## References

[1] A.R. Petcu, C.A. Lazar, E.A. Rogozea, N.L. Olteanu, A. Meghea, M. Mihaly, Nonionic microemulsion systems applied for removal of ionic dyes mixtures from textile industry wastewaters, Sep. Purif. Technol., 158 (2016) 155–159.
[2] D.A. Yaseen, M. Scholz, Textile dye wastewater characteristics and constituents of synthetic effluents: a critical review, Int. J. Environ. Sci. Technol., 16 (2019) 1193–1226.
[3] H.B. Slama, A. Chenari Bouket, Z. Pourhassan, F.N. Alenezi, A. Silini, H. Cherif-Silini, T. Oszako, L. Luptakova, P. Golińska, L. Belbahri, Diversity of synthetic dyes from textile industries, discharge impacts and treatment methods, Appl. Sci., 11 (2021), doi: 10.3390/app11146255.
[4] S. Dutta, B. Gupta, S.K. Srivastava, A.K. Gupta, Recent advances on the removal of dyes from wastewater using various adsorbents: a critical review, Mater. Adv., 2 (2021) 4497–4531.
[5] T. Shindhal, P. Rakholiya, S. Varjani, A. Pandey, H.H. Ngo, W. Guo, H.Y. Ng, M.J. Taherzadeh, A critical review on advances in the practices and perspectives for the treatment of dye industry wastewater, Bioengineered, 12 (2021) 70–87.
[6] B. Lellis, C.Z. Fávaro-Polonio, J.A. Pamphile, J.C. Polonio, Effects of textile dyes on health and the environment and bioremediation potential of living organisms, Biotechnol. Res. Innov., 3 (2019) 275–290.
[7] J. Mittal, Permissible synthetic food dyes in india, Resonance, 25 (2020) 567–577.
[8] C.R. Holkar, A.J. Jadhav, D.V. Pinjari, N.M. Mahamuni, A.B. Pandit, A critical review on textile wastewater treatments: possible approaches, J. Environ. Manage., 182 (2016) 351–366.
[9] D. Bhatia, N.R. Sharma, J. Singh, R.S. Kanwar, Biological methods for textile dye removal from wastewater: a review, Crit. Rev. Env. Sci. Technol., 47 (2017) 1836–1876.
[10] B.L. Alderete, J. da Silva, R. Godoi, F.R. da Silva, S.R. Taffarel, L.P. da Silva, A.L.H. Garcia, H.M. Júnior, H.L.N. de Amorim, J.N. Picada, Evaluation of toxicity and mutagenicity of a synthetic effluent containing azo dye after advanced oxidation process treatment, Chemosphere., 263 (2021) 128291, doi: 10.1016/j.chemosphere.2020.128291.

[11] A. Patel, S. Soni, J. Mittal, A. Mittal, C. Arora, Sequestration of crystal violet from aqueous solution using ash of black turmeric rhizome, Desal. Water Treat., 220 (2021) 342–352.
[12] C. Aroraa, P. Kumar, S. Soni, J. Mittal, A. Mittal, B. Singh, Efficient removal of malachite green dye from aqueous solution using *Curcuma caesia* based activated carbon, Desal. Water Treat., 195 (2020) 341–352.
[13] H. Daraeia, A. Mittal, Investigation of adsorption performance of activated carbon prepared from waste tire for the removal of methylene blue dye from wastewater, Desal. Water Treat., 90 (2017) 294–298.
[14] A. Mariyam, J. Mittal, F. Sakina, R.T. Baker, A.K. Sharma, A. Mittal, Efficient batch and fixed-bed sequestration of a basic dye using a novel variant of ordered mesoporous carbon as adsorbent, Arabian J. Chem., 14 (2021) 103186, doi: 10.1016/j.arabjc.2021.103186.
[15] J. Mittal, A. Mariyam, F. Sakina, R.T. Baker, A.K. Sharma, A. Mittal, Batch and bulk adsorptive removal of anionic dye using metal/halide-free ordered mesoporous carbon as adsorbent, J. Cleaner Prod., 321 (2021) 129060, doi: 10.1016/j.jclepro.2021.129060.
[16] M. Ayisha Sidiqua, V.S. Priya, Removal of yellow dye using composite binded adsorbent developed using natural clay and activated carbon from sapindus seed, Biocatal. Agric. Biotechnol., 33 (2021) 101965, doi: 10.1016/j.bcab.2021.101965.
[17] L. Baloo, M.H. Isa, N. Bin Sapari, A.H. Jagaba, L.J. Wei, S. Yavari, R. Razali, R. Vasu, Adsorptive removal of methylene blue and acid orange 10 dyes from aqueous solutions using oil palm wastes-derived activated carbons, Alexandria Eng. J., 60 (2021) 5611–5629.
[18] C. Osagie, A. Othmani, S. Ghosh, A. Malloum, Z. Kashitarash Esfahani, S. Ahmadi, Dyes adsorption from aqueous media through the nanotechnology: a review, J. Mater. Res. Technol., 14 (2021) 2195–2218.
[19] O. Moradi, G. Sharma, Emerging novel polymeric adsorbents for removing dyes from wastewater: a comprehensive review and comparison with other adsorbents, Environ. Res., 201 (2021) 111534, doi: 10.1016/j.envres.2021.111534.
[20] M. Paredes-Laverde, M. Salamanca, J.D. Diaz-Corrales, E. Flórez, J. Silva-Agredo, R.A. Torres-Palma, Understanding the removal of an anionic dye in textile wastewaters by adsorption on $ZnCl_2$ activated carbons from rice and coffee husk wastes: a combined experimental and theoretical study, J. Environ. Chem. Eng., 9 (2021) 105685, doi: 10.1016/j.jece.2021.105685.
[21] Aruna, N. Bagotia, A.K. Sharma, S. Kumar, A review on modified sugarcane bagasse biosorbent for removal of dyes, Chemosphere, 268 (2021) 129309, doi: 10.1016/j.chemosphere.2020.129309.
[22] P.R. Yaashikaa, P.S. Kumar, A. Saravanan, D.-V.N. Vo, Advances in biosorbents for removal of environmental pollutants: a review on pretreatment, removal mechanism and future outlook, J. Hazard. Mater., 420 (2021) 126596, doi: 10.1016/j.jhazmat.2021.126596.
[23] M. Kurakula, S. Gorityala, K. Moharir, Recent trends in design and evaluation of chitosan-based colon targeted drug delivery systems: update 2020, J. Drug Delivery Sci. Technol., 64 (2021) 102579, doi: 10.1016/j.jddst.2021.102579.
[24] D.C. da Silva Alves, B. Healy, L.A. de A. Pinto, T.R.S. Cadaval, C.B. Breslin, Recent developments in chitosan-based adsorbents for the removal of pollutants from aqueous environments, Molecules, 26 (2021), doi: 10.3390/molecules26030594.
[25] N. Aramesh, A.R. Bagheri, M. Bilal, Chitosan-based hybrid materials for adsorptive removal of dyes and underlying interaction mechanisms, Int. J. Biol. Macromol., 183 (2021) 399–422.
[26] I.O. Saheed, W. Da Oh, F.B.M. Suah, Chitosan modifications for adsorption of pollutants – a review, J. Hazard. Mater., 408 (2021) 124889, doi: 10.1016/j.jhazmat.2020.124889.
[27] T.H.A. Nguyen, T.D.M. Tran, T. Ky Vo, Q.T. Nguyen, V.-C. Nguyen, Facile synthesis of low-cost chitosan/$Fe_3O_4$@C composite for highly efficient adsorption of levofloxacin antibiotic, Chem. Eng. Commun., (2022) 1–13, doi: 10.1080/00986445.2022.2053680.
[28] J. Liu, H.-T. Wu, J. Lu, X. Wen, J. Kan, C. Jin, Preparation and characterization of novel phenolic acid (hydroxybenzoic and hydroxycinnamic acid derivatives) grafted chitosan microspheres with enhanced adsorption properties for Fe(II), Chem. Eng. J., 262 (2015) 803–812.
[29] S.-T. Ong, C.-K. Seou, Removal of reactive black 5 from aqueous solution using chitosan beads: optimization by Plackett–Burman design and response surface analysis, Desal. Water Treat., 52 (2014) 7673–7684.
[30] S. Karmaker, A.J. Nag, T.K. Saha, Adsorption of Reactive Blue 4 dye onto Chitosan 10B in aqueous solution: kinetic modeling and isotherm analysis, Russ. J. Phys. Chem. A, 94 (2020) 2349–2359.
[31] H. Karaer, İ. Kaya, Synthesis, characterization of magnetic chitosan/active charcoal composite and using at the adsorption of methylene blue and reactive blue4, Microporous Mesoporous Mater., 232 (2016) 26–38.
[32] A. Samadi, M. Xie, J. Li, H. Shon, C. Zheng, S. Zhao, Polyaniline-based adsorbents for aqueous pollutants removal: a review, Chem. Eng. J., 418 (2021) 129425, doi: 10.1016/j.cej.2021.129425.
[33] I.M. Minisy, N.A. Salahuddin, M.M. Ayad, Adsorption of methylene blue onto chitosan–montmorillonite/polyaniline nanocomposite, Appl. Clay Sci., 203 (2021) 105993, doi: 10.1016/j.clay.2021.105993.
[34] T.N.M. An, T.T. Phuc, D.N.T. Nhi, N. Van Cuong, Removal of reactive red dye by reusable chitosan-polyaniline/$Fe_3O_4$ nanocomposite, Vietnam J. Chem., 58 (2020) 477–481.
[35] M. Ahiduzzaman, A.K.M.S. Islam, Preparation of porous bio-char and activated carbon from rice husk by leaching ash and chemical activation, Springerplus, 5 (2016) 1–14.
[36] B.S. Todkar, O.A. Deorukhkar, S.M. Deshmukh, Extraction of silica from rice husk, Int. J. Eng. Res. Dev., 12 (2016) 69–74.
[37] R. Wu, J.H. Liu, L. Zhao, X. Zhang, J. Xie, B. Yu, X. Ma, S.T. Yang, H. Wang, Y. Liu, Hydrothermal preparation of magnetic $Fe_3O_4$@C nanoparticles for dye adsorption, J. Environ. Chem. Eng., 2 (2014) 907–913.
[38] M. Fernandes Queiroz, K.R.T. Melo, D.A. Sabry, G.L. Sassaki, H.A.O. Rocha, Does the use of chitosan contribute to oxalate kidney stone formation?, Mar. Drugs, 13 (2015) 141–158.
[39] K.A. Ibrahim, Synthesis and characterization of polyaniline and poly (aniline-co-o-nitroaniline) using vibrational spectroscopy, Arabian J. Chem., 10 (2017) S2668–S2674.
[40] B. Mohammadi, S. Pirsa, M. Alizadeh, Preparing chitosan–polyaniline nanocomposite film and examining its mechanical, electrical, and antimicrobial properties, Polym. Polym. Compos., 27 (2019) 507–517.
[41] B.S. Rathore, N.P.S. Chauhan, M.K. Rawal, S.C. Ameta, R. Ameta, Chitosan–polyaniline–copper(II) oxide hybrid composite for the removal of methyl orange dye, Polym. Bull., 77 (2020) 4833–4850.
[42] S.T. Danalıoğlu, Ş.S. Bayazit, Ö. Kerkez Kuyumcu, M.A. Salam, c antibiotics by a novel magnetic adsorbent: magnetic activated carbon/chitosan (MACC) nanocomposite, J. Mol. Liq., 240 (2017) 589–596.
[43] V.C. Nguyen, T.M.D. Luu, T.O. Nguyen, Reusable mn-doped ZnS magnetic nanocomposite for photodegradation of textile dyes, J. Nano Res., 33 (2015) 72–82.
[44] S. Sahnoun, M. Boutahala, Adsorption removal of tartrazine by chitosan/polyaniline composite: kinetics and equilibrium studies, Int. J. Biol. Macromol., 114 (2018) 1345–1353.
[45] M.N. Ahmad, A. Hussain, M.N. Anjum, T. Hussain, A. Mujahid, M. Hammad Khan, T. Ahmed, Synthesis and characterization of a novel chitosan-grafted-polyorthoethylaniline biocomposite and utilization for dye removal from water, Open Chem., 18 (2020) 843–849.
[46] V. Janaki, B.-T. Oh, K. Shanthi, K.-J. Lee, A.K. Ramasamy, S. Kamala-Kannan, Polyaniline/chitosan composite: an eco-friendly polymer for enhanced removal of dyes from aqueous solution, Synth. Met., 162 (2012) 974–980.
[47] N.U.M. Nizam, M.M. Hanafiah, E. Mahmoudi, A.A. Halim, A.W. Mohammad, The removal of anionic and cationic dyes from an aqueous solution using biomass-based activated carbon, Sci. Rep., 11 (2021) 8623, doi: 10.1038/s41598-021-88084-z.

[48] S. Razzaq, M. Akhtar, S. Zulfiqar, S. Zafar, I. Shakir, P.O. Agboola, S. Haider, M.F. Warsi, Adsorption removal of Congo red onto L-cysteine/rGO/PANI nanocomposite: equilibrium, kinetics and thermodynamic studies, J. Taibah Univ. Sci., 15 (2021) 50–62.
[49] P. Vairavel, N. Rampal, G. Jeppu, Adsorption of toxic Congo red dye from aqueous solution using untreated coffee husks: kinetics, equilibrium, thermodynamics and desorption study, Int. J. Environ. Anal. Chem., (2021) 1–20, doi: 10.1080/03067319.2021.1897982.
[50] S. Hussain, M. Kamran, S.A. Khan, K. Shaheen, Z. Shah, H. Suo, Q. Khan, A.B. Shah, W.U. Rehman, Y.O. Al-Ghamdi, U. Ghani, Adsorption, kinetics and thermodynamics studies of methyl orange dye sequestration through chitosan composites films, Int. J. Biol. Macromol., 168 (2021) 383–394.
[51] M. Hosseinzehi, M. Khatebasreh, A. Dalvand, Modeling of Reactive Black 5 azo dye adsorption from aqueous solution on activated carbon prepared from poplar sawdust using response surface methodology, Int. J. Environ. Anal. Chem., (2020) 1–18, doi: 10.1080/03067319.2020.1819991.
[52] N.N.A. Malek, A.H. Jawad, K. Ismail, R. Razuan, Z.A. ALOthman, Fly ash modified magnetic chitosan-polyvinyl alcohol blend for reactive orange 16 dye removal: adsorption parametric optimization, Int. J. Biol. Macromol., 189 (2021) 464–476.
[53] H.T. Van, L.H. Nguyen, N.V. Dang, H.-P. Chao, Q.T. Nguyen, T.H. Nguyen, T.B.L. Nguyen, D. Van Thanh, H.D. Nguyen, P.Q. Thang, P.T.H. Thanh, V.P. Hoang, The enhancement of reactive red 24 adsorption from aqueous solution using agricultural waste-derived biochar modified with ZnO nanoparticles, RSC Adv., 11 (2021) 5801–5814.
[54] V.S. Munagapati, J.-C. Wen, C.-L. Pan, Y. Gutha, J.-H. Wen, Enhanced adsorption performance of Reactive Red 120 azo dye from aqueous solution using quaternary amine modified orange peel powder, J. Mol. Liq., 285 (2019) 375–385.
[55] M. Malakootian, H.J. Mansoorian, A. Hosseini, N. Khanjani, Evaluating the efficacy of alumina/carbon nanotube hybrid adsorbents in removing Azo Reactive Red 198 and Blue 19 dyes from aqueous solutions, Process Saf. Environ. Prot., 96 (2015) 125–137.
[56] H.-A. Tayebi, Z. Dalirandeh, A. Shokuhi Rad, A. Mirabi, E. Binaeian, Synthesis of polyaniline/$Fe_3O_4$ magnetic nanoparticles for removal of reactive red 198 from textile waste water: kinetic, isotherm, and thermodynamic studies, Desal. Water Treat., 57 (2016) 22551–22563.
[57] B. Liu, D. Wang, X. Gao, L. Zhang, Y. Xu, Y. Li, Removal of arsenic from *Laminaria japonica* Aresch juice using As(III)-imprinted chitosan resin, Eur. Food Res. Technol., 232 (2011) 911.
[58] S.Y. Tay, V.L. Wong, S.S. Lim, I.L.R. Teo, Adsorption equilibrium, kinetics and thermodynamics studies of anionic methyl orange dye adsorption using chitosan-calcium chloride gel beads, Chem. Eng. Commun., 208 (2021) 708–726.

## Supplementary information

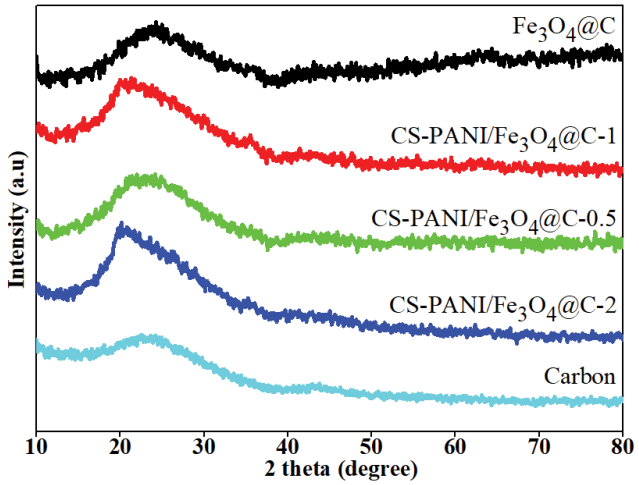


Fig. S1. XRD pattern of carbon, $Fe_3O_4$@C, CS-PANI/$Fe_3O_4$@C-2, CS-PANI/$Fe_3O_4$@C-1, and CS-PANI/$Fe_3O_4$@C-0.5.

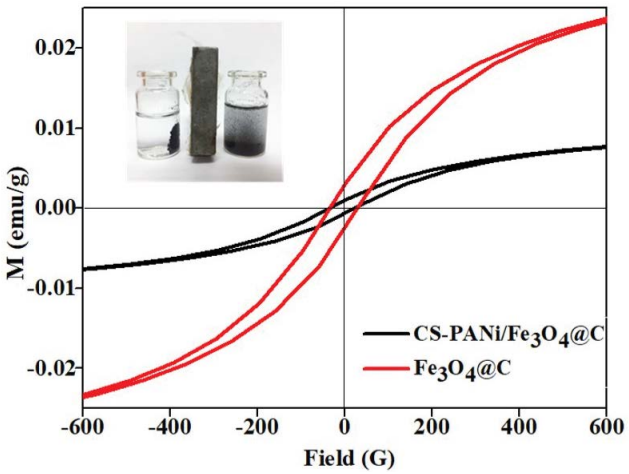


Fig. S2. VSM of CS-PANi/$Fe_3O_4$@C composite and $Fe_3O_4$@C. Insert: adsorbent in the presence of magnet.